*Desalination and Water Treatment*
www.deswater.com
doi: 10.1080/19443994.2016.1204561

57 (2016) 29404–29410
December

Taylor & Francis
Taylor & Francis Group

# Preparation, physicochemical, and electrochemical properties of magnetite electrodes for methanol electrocatalytic oxidation in an alkaline medium

Cheng-Di Dong, Chiu-Wen Chen, Chang-Mao Hung*

*Department of Marine Environmental Engineering, National Kaohsiung Marine University, 142 Haijhuan Road, Nanzih District, Kaohsiung City 81157, Taiwan, Tel. +886 7 3617141, ext. 3762; email: cddong@mail.nkmu.edu.tw (C.-D. Dong), Tel. +886 7 3617141, ext. 3761; email: cwchen@mail.nkmu.edu.tw (C.-W. Chen), Tel. +886 7 3617141, ext. 3777; Fax: +886 7 3650548; email: hungcm1031@gmail.com (C.-M. Hung)*

Received 26 October 2015; Accepted 17 June 2016

ABSTRACT

Iron oxide nanoparticles are novel functional materials applicable in catalysis. Herein, the proposed method involved synthesis of electrocatalyst iron oxide nanoparticles and their application in oxidation process of methanol. The iron oxide nanoparticles prepared using co-precipitation chemical method, in which ferric and ferrous ions were mixed in a 1:2 M ratio in highly basic solutions. The electrocatalyst $Fe_3O_4$ further applied for methanol oxidation reaction (MOR) in 0.5 M KOH solution at room temperature. MOR was performed on cyclic voltammeter (CV) also measured polarization of process. The methanol oxidation on cyclic voltammetry expressed forward and backward oxidation peak with function of currents at 0.7 and 0.5 V. The prepared $Fe_3O_4$ nanoparticles showed significant magnetic property measured by a vibration magnetometer at 300 K. Also, the structure and surface morphology of the catalyst were characterized using X-ray diffraction and environmental scanning electron microscopy (ESEM)–energy dispersive spectroscopy, respectively. ESEM was used to determine $Fe_3O_4$ particle size and a high degree of nanoparticle dispersion in oxidation system.

*Keywords:* Electrochemical oxidation; Methanol; Magnetite electrocatalyst; Cyclic voltammetry

## 1. Introduction

At present, methanol ($CH_3OH$) has attracted increasing attention worldwide because of its high-power density, energy conversion efficiency, low-pollution emissions, etc. [1]. To increase the electrocatalytic oxidation of $CH_3OH$, many researchers reported application of novel catalyst with high electrocatalytic activity. In addition, it targets to potentially shorten the oxidation time and allow reaction process under mild operating conditions inside fuel cells. From an energetic and ecological perspective, the electrocatalytic oxidation of $CH_3OH$ into a stream of $H_2$ is intriguing because this reaction is appropriate for developing suitable catalytic materials and

---

*Corresponding author.

*Presented at the 8th International Conference on Challenges in Environmental Science & Engineering (CESE-2015)*
*28 September–2 October 2015, Sydney, Australia*

technologies for reducing the $CH_3OH$ crossover effect [2]. At present, practical catalyst for such type of reaction is carried out by platinum-based materials, whereas $H_2$ represents a promising fuel for proton exchange membrane fuel cells as well as environmental friendly. The major drawbacks of platinum-based method were the formation of the poisonous intermediates, limited resources, and expensive [3,4]. In advance, oxides were utilized with Pt nanoparticles attached to grapheme-encapsulated magnetite ($Fe_3O_4$), with oxidation of methanol in $H_2SO_4$ resulted with improved method [5,6]. These methods principally based on oxygen–reduction reaction (ORR) were usually involved in electrochemical reaction carried out in fuel cells, which enabled feasible methanol oxidation reaction (MOR) process. Afterwards Guo et al. [7], Sun et al. [8], and Huang research groups [9] developed methanol oxidation methods with best design, heterogenous non-precious composite fuel cells.

Among them $Fe_3O_4$ nanoparticles demonstrated selective catalytic and oxidation–reduction potential [10,11]. In addition, an electrical and magnetic property enhances methanol conversion efficiency and increased intermediate (CO) tolerance [12]. Therefore, some studies had been applied to $Fe_3O_4$ to determine the reactive characteristics of the active materials during the electricatalytic liquid-phase oxidation of $CH_3OH$ [13–15]. We reported an improved significant electrocatalytic oxidation technique for MOR with $Fe_3O_4$ activity in alkaline medium using cyclic voltammetry. The catalyst i.e. iron oxide nanoparticle was characterized by polarization, vibrating sample magnetometry spectroscopy, X-ray diffraction (XRD) and environmental scanning electron microscopy (ESEM).

## 2. Materials and methods

### 2.1. Catalyst preparation

Magnetic particles ($Fe_3O_4$) were prepared through the chemical co-precipitation of $FeCl_3{\cdot}6H_2O$ and $FeCl_2{\cdot}4H_2O$ in 1:2 M ratio in deionized water [16]. The precipitates were thoroughly stirred and $NH_4OH$ was dropwise added with continuous stirring until pH >9.0 was attained at room temperature (~30 min). Afterwards, the reaction mixture was heated at 353 K for 4 h. The resulting precipitates were washed with DI water and freeze-dried for further experiment. The resulting particles were black in color with strong magnetic response. The chemical reaction involved in the formation of $Fe_3O_4$ co-precipitation is as follows:

$$Fe^{2+} + 2Fe^{3+} + 8OH^- \rightarrow Fe_3O_4 + 4H_2O \qquad (1)$$

All the reagents used in the experiment were of analytical grade without further purification. Deionized water was used for solution preparation throughout the entire experiment.

### 2.2. Experimental procedure

Cyclic voltammograms were recorded at room temperature with an electrochemical analyzer (CHI 6081D, USA) equipped with three-electrode electrochemical cells to investigate the electrochemical behaviors of electrode samples. A glassy carbon (GC) electrode (diameter, 3 mm; CHI 104, USA) loaded with active $Fe_3O_4$ samples was used as the working electrode and scanned at 5, 10, 50, and 100 mV $s^{-1}$, while the potential was cycled between −0.2 and 1.2 V. A Pt wire (CHI 102, USA) and a standard hydrogen electrode were used as the counter electrode (CE) and reference electrode (RE), respectively. Before CV measurements, the electrolyte solution, i.e. 0.5 M KOH, was degassed by bubbling with $N_2$. XRD analysis was performed on a Diano-8536 diffractometer equipped with a Cu Kα radiation source. During analyses, samples were scanned from 20° to 80° at $0.4^\circ\,min^{-1}$. Magnetic measurements of the samples were performed using a superconducting quantum interference device magnetometer (MPMS-XL7, Quantum Design, USA). The morphology and structure of catalyst ($Fe_3O_4$) were studied by ESEM system equipped with an EDS X-ray spectrometer (Quanta 200 FEG, FEI Company, Czech Republic).

## 3. Results and discussions

The CV curves at different scan rates (5–100 mV $s^{-1}$) in 0.5 M KOH are plotted in Fig. 1. Typical $H_2$ desorption peaks from $Fe_3O_4$ are observed in the potential region of −0.2 to 0.15 V. The $Fe_3O_4$ electrocatalyst displayed little reactivity in the potential window when the scan rates were 5 and 10 mV $s^{-1}$. The CV curves revealed the superior reduction capacity because well-marked oxidation peaks appeared at 0.55 V which are attributable to the reduction of $Fe^{3+}$ to $Fe^{2+}$ in $Fe_3O_4$ and the irreversible reaction associated with electrolyte decomposition and increased the electrolyte's current density under higher potential scan rates (50 and 100 mV $s^{-1}$) [17]. These results similarly agree with an earlier study proposed by Yin research group [18]. The increase in current density that occurred when the potential scan rate increased is attributable to the charged interface capacitance caused by charge transfer [19]. Vot et al. [20] investigated electrochemical oxidation for

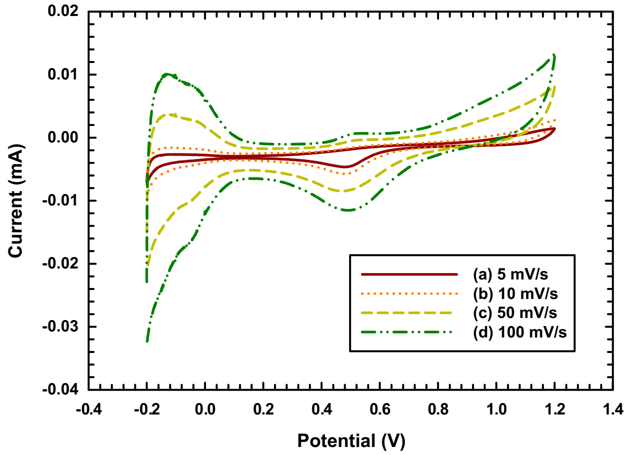

Fig. 1. Cyclic voltammogram profiles in a 0.5 M KOH solution recorded at various scan rates for the $Fe_3O_4$ electrocatalyst.

characterizing $H_2$ adsorption–desorption (between −0.2 and 0.2 V) and double-layer (between 0.2 and 0.6 V) regions through CV. Compared with our findings, the electrochemical behavior of the catalyst was associated with both $CH_3OH$ oxidation and surface composition of the catalyst.

The characteristics of electrocatalyst ($Fe_3O_4$) were crucial factor before performing oxidation–reduction reaction in this experiment. Fig. 2 shows the CV profiles at scan rates from 5 to 100 mV s$^{-1}$ for $Fe_3O_4$ electrocatalyst with 0.5 M $CH_3OH$ added to 0.5 M KOH. Electro-oxidation was not observed at bare unmodified GC electrode at alkaline medium so that the modified electrode with catalyst used for the oxidation of $CH_3OH$ [21]. The metal oxidation–reduction occurred in the range of 0.4–0.9 V, where the redox process of $Fe_3O_4$ can be observed. Fig. 2 shows that until ~0.5 V oxidation current density was not observed. While scanning at 10, 50, and 100 mV s$^{-1}$ $CH_3OH$ adsorption at the electrode surface hindered hydroxyl ion or oxide layer formation on the catalyst, thus altering the electrode–electrolyte interfacial properties in the solution. Furthermore, the CV plots revealed that the $Fe_3O_4$ electrocatalyst had forward and backward oxidation peak currents at 0.7 and 0.5 V, respectively. This reactivity pattern may indicate the catalytic redox cycling of Fe by reducing Fe(III) to Fe(II), thus accelerating $CH_3OH$ oxidation. The peak currents of the wave increased linearly with the potential scan rate, which is typical of the Fe(III)–Fe(II) reaction of an electrode surface-adsorbed redox couple [15,22]. Subsequently, during alcohol oxidation reaction, $O_2$-containing species could more easily form on the surface of oxides, which reacted with CO-like intermediate species on oxides to produce $CO_2$ or other dissolvable products and release the active sites for further electrochemical reaction, which can catalyze ORR [2]. Moreover, $Fe_3O_4$ functioned as an $O_2$ activator to produce the –OH species required to oxidize $CO_{ads}$ into $CO_2$ at the active sites during the alcohols oxidation reaction [11]. Furthermore, the catalytic activity may have been strengthened by the strong interaction among $Fe_3O_4$ particles. The $Fe_3O_4$ electrocatalytic materials scanned at 5 and 10 mV s$^{-1}$ exhibited a decrease in $CH_3OH$ oxidation peak currents in the given potential window (Fig. 2). The oxidation peak in the reverse sweep is according to the poisoning and structural change in $Fe_3O_4$ because of disruption of the potential during scanning in an aqueous solution [2].

To elucidate the corrosion properties of the complex $Fe_3O_4$ electrocatalyst, we conducted experiments in 0.5 M KOH using polarization curve profiles and performed MOR in an alkaline medium using the equilibrium potential $V_{eq}$ (Fig. 3). In 0.5 M KOH, the $Fe_3O_4$ electrocatalyst generated a shoulder peak at approximately 1.18 V in the potential window, shown as the equilibrium potential $V_{eq}$ in Fig. 3. Moreover, the polarization curve plots revealed that in 0.5 M $CH_3OH$, the $Fe_3O_4$ electrocatalyst generated a prominent potential peak at 1.2 V, which is near the corrosion potential of the catalyst (Fig. 3). This was proposed on the basis of the cycle of redox pairs of $Fe^{3+}/Fe^{2+}$ catalyzed by alcohol species and electron transfer from an excited $CH_3OH$ molecule to $Fe^{3+}$ [23].

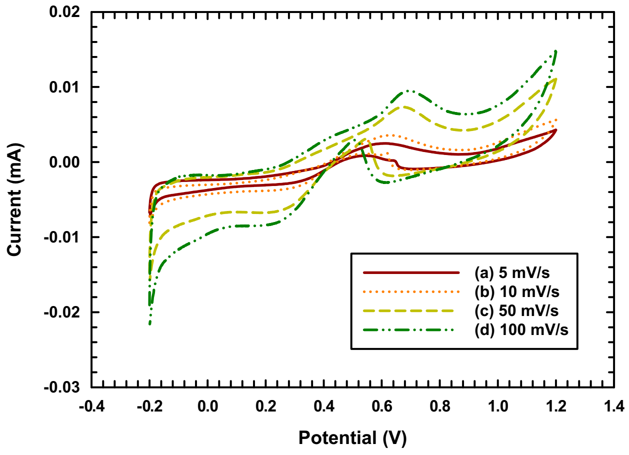

Fig. 2. Cyclic voltammograms profiles in a 0.5 M KOH plus 0.5 M $CH_3OH$ solution electrocatalytically recorded at various scan rates for the $Fe_3O_4$ electrocatalyst.

Fig. 4 shows the XRD patterns of fresh and used catalyst and shows that the catalyst changed during exposure to the catalytic environment. Furthermore,

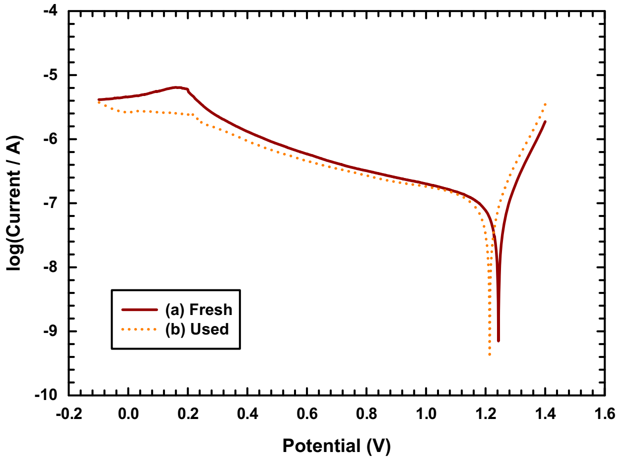

Fig. 3. Polarization curves of the $Fe_3O_4$ electrocatalyst in a 0.5 M KOH plus 0.5 M $CH_3OH$ solution (a) before and (b) after the electrocatalytic test.

XRD analysis confirmed the presence of $Fe_3O_4$ in the catalyst. The XRD patterns of freshly prepared $Fe_3O_4$ and used $Fe_3O_4$ after MOR were similar. The dominant $Fe_3O_4$ diffraction peaks detected at $2\theta$ values of approximately 18.3°, 30.2°, 35.4°, 37.2°, 43.2°, 53.7°, 57.3°, 62.8°, and 74.2° were associated with the (1 1 1), (2 2 0), (3 1 1), (2 2 2), (4 0 0), (4 2 2), (5 1 1), (4 4 0), and (5 3 3) planes, respectively. Therefore, the diffraction peaks of nanoparticles closely matched those of $Fe_3O_4$, confirming the cubic spinel-type phase of the samples. This result agrees well with those of previous studies [5,24]. The XRD results indicated that $Fe_3O_4$ active sites were formed on the $Fe_3O_4$ catalyst. Therefore, $CH_3OH$ was probably adsorbed on the catalyst surface before undergoing a catalytic reaction at the $Fe_3O_4$ active sites.

Fig. 5 shows the magnetic hysteresis loops of fresh and used $Fe_3O_4$ samples with a magnetic field cycle between −10 and +10 kOe at 300 K. Both the fresh and used samples were magnetic at room temperature, and the $M$–$H$ hysteresis curves passed the original spot, revealing the super paramagnetic nature of magnetic $Fe_3O_4$ materials. The saturation magnetization ($M_S$) of the fresh and used samples was 88 emu $g^{-1}$, and it gradually decreased to 78 emu $g^{-1}$ because of the over-oxidation of $Fe_3O_4$ after the activity test. However, the observed $M_S$ value of $Fe_3O_4$ (88 emu $g^{-1}$) was similar to previously reported method [5].

Fig. 6 presents the changes in the surface morphology and structure of the $Fe_3O_4$ catalyst, as elucidated by ESEM. These data provide crucial information regarding the catalyst surface structure during $CH_3OH$ oxidation. The agglomerates observed through ESEM indicated that the composite catalyst particles formed fine grains and prickly sphere-like iron oxide species (Fig. 6). However, Fig. 6(a) also revealed that the catalyst surface was more mono-dispersed and well-crystallized than the surface shown in Fig. 6(b). These small crystalline phases indicate that the high catalytic activity may be due to the highly dispersed nanoscale particles (~approximately 100 nm). Specifically, disaggregated phases formed as the catalyst surface aged or poisoned through plugging, implying that the porosity of particles had changed (Fig. 6). Moreover, this change in porosity might explain the increased over-potential of the catalytic reaction and therefore the decline in the $CH_3OH$

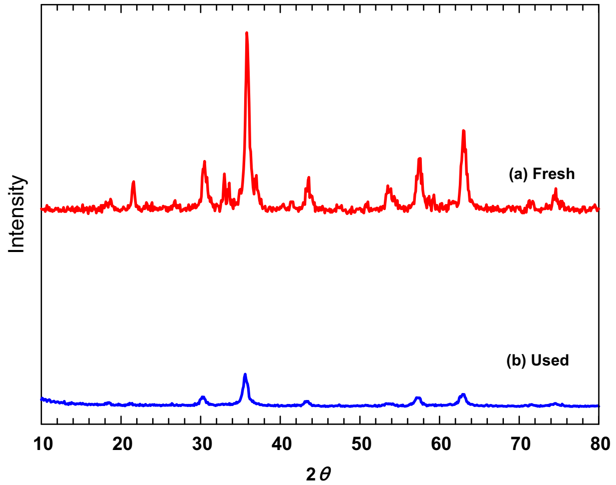

Fig. 4. XRD patterns of the $Fe_3O_4$ electrocatalyst in a 0.5 M KOH plus 0.5 M $CH_3OH$ solution (a) before and (b) after the electrocatalytic test.

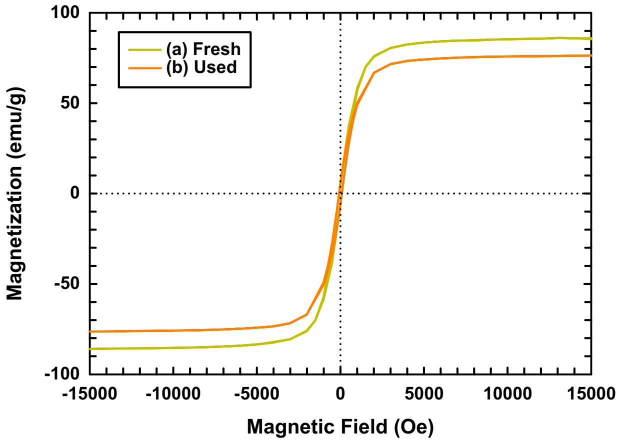

Fig. 5. Magnetic hysteresis loops (at 300 K) of the $Fe_3O_4$ electrocatalyst in a 0.5 M KOH plus 0.5 M $CH_3OH$ solution (a) before and (b) after the electrocatalytic test.

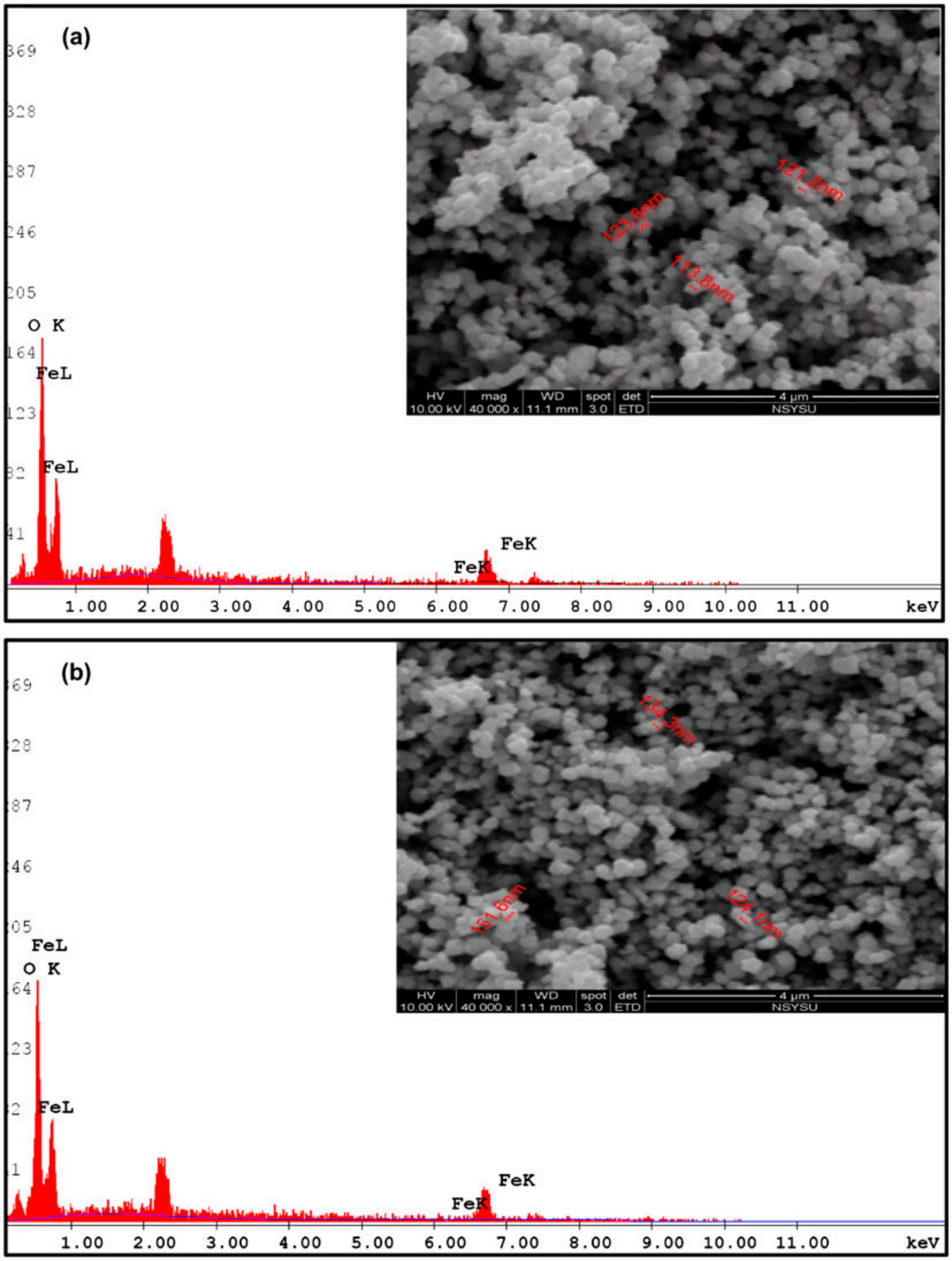

Fig. 6. ESEM–EDS images of the $Fe_3O_4$ electrocatalyst in a 0.5 M KOH plus 0.5 M $CH_3OH$ solution (a) before and (b) after the electrocatalytic test.

oxidation performance. Consequently, the electrocatalytic activity of the prepared $Fe_3O_4$ catalyst for $CH_3OH$ oxidation in aqueous solutions is dependent on the surface crystalline phases of the particles.

## 4. Conclusions

Here, we reported a simple method for preparation of $Fe_3O_4$ catalyst and tested it for the electro-oxidation of $CH_3OH$ in an alkaline solution. The surface peak current density and potential electrochemical characterizations of $Fe_3O_4$ electrocatalytic materials considerably enhanced catalytic performance during MOR. Their electrochemical behavior was investigated through cyclic voltammetry. The wide current density peak for $CH_3OH$ oxidation proved that catalyst exhibited excellent activity across a wide potential range. The $Fe_3O_4$ electrocatalyst underwent further reduction at higher potential scan rates. Therefore, the electrocatalyst is necessary during the $CH_3OH$ electrocatalytic process. Because of the magnetic property of $Fe_3O_4$ nanoparticles, $Fe_3O_4$ can be readily manipulated by a magnetic field and used products can be recycled. This strategy of cost-effective fabrication of $Fe_3O_4$ electrocatalysts facilitates the development of various metal oxide nanocomposites for constructing high-performance electro-oxidation materials.

## Acknowledgment

The authors thank the National Science Council of the Republic of China, Taiwan, for financially supporting this research under contract numbers MOST 103-2221-E-022-001-MY3 and MOST 103-2811-E-022-002.

## References

[1] S.H. Liu, W.Y. Yu, C.H. Chen, A.Y. Lo, B.J. Hwang, S.H. Chien, S.B. Liu, Fabrication and characterization of well-dispersed and highly stable PtRu nanoparticles on carbon mesoporous material for applications in direct methanol fuel cell, Chem. Mater. 20 (2008) 1622–1628.

[2] J. Li, J. Ren, G. Yang, P. Wang, H. Li, X. Sun, L. Chen, J.T. Ma, R. Li, Simple and efficient deposition of Pd nanoparticles on $Fe_3O_4$ hollow nanospheres: A new catalytic system for methanol oxidation in alkaline media, Mater. Sci. Eng.: B 172 (2010) 207–212.

[3] C.D. Dong, C.W. Chen, C.F. Chen, C.M. Hung, Platinum particles supported on mesoporous carbons: Fabrication and electrocatalytic performance in methanol-tolerant oxygen-reduction reactions, Sci. Reports 4 (2014) 1–8.

[4] K.H. Ye, S.A. Zhou, X.C. Zhu, C.W. Xu, P.K. Shen, Stability analysis of oxide ($CeO_2$, NiO, $Co_3O_4$ and $Mn_3O_4$) effect on Pd/C for methanol oxidation in alkaline medium, Electrochim. Acta 90 (2013) 108–111.

[5] S. Lin, C. Shen, D. Lu, C. Wang, H.J. Gao, Synthesis of Pt nanoparticles anchored on graphene encapsulated $Fe_3O_4$ magnetic nanospheres and their use as catalysts for methanol oxidation, Carbon 53 (2013) 112–119.

[6] S. Guo, S. Zhang, D. Su, S. Sun, Seed-mediated synthesis of core/shell FePtM/FePt (M = Pd, Au) nanowires and their electrocatalysis for oxygen reduction reaction, J. Am. Chem. Soc. 135 (2013) 13879–13884.

[7] S. Guo, S. Zhang, X. Sun, S. Sun, Synthesis of ultrathin FePtPd nanowires and their use as catalysts for methanol oxidation reaction, J. Am. Chem. Soc. 133 (2011) 15354–15357.

[8] H. Sun, J. You, M. Yang, F. Qu, Synthesis of Pt/$Fe_3O_4$–$CeO_2$ catalyst with improved electrocatalytic activity for methanol oxidation, J. Power Sources 205 (2012) 231–234.

[9] D. Huang, Y. Luo, S. Li, M. Wang, Y. Shen, Hybrid of Fe@$Fe_3O_4$ core–shell nanoparticle and iron-nitrogen-doped carbon material as an efficient electrocatalyst for oxygen reduction reaction, Electrochim. Acta 174 (2015) 933–939.

[10] Y. Ma, H. Wang, J. Key, V. Linkov, S. Ji, X. Mao, Q. Wang, R. Wang, Ultrafine iron oxide nanoparticles supported on N-doped carbon black as an oxygen reduction reaction catalyst, Int. J. Hydrogen Energy 39 (2014) 14777–14782.

[11] N.M. Sánchez-Padilla, S.M. Montemayor, L.A. Torres, F.J. Rodríguez Varela, Fast synthesis and electrocatalytic activity of M@Pt (M = Ru, $Fe_3O_4$, Pd) core–shell nanostructures for the oxidation of ethanol and methanol, Int. J. Hydrogen Energy 38 (2013) 12681–12688.

[12] H. Yang, H. Wang, S. Ji, V. Linkov, R. Wang, Synergy between isolated-$Fe_3O_4$ nanoparticles and $CN_x$ layers derived from lysine to improve the catalytic activity for oxygen reduction reaction, Int. J. Hydrogen Energy 39 (2014) 3739–3745.

[13] K. Routray, W. Zhou, C.J. Kiely, I.E. Wachs, Catalysis science of methanol oxidation over iron vanadate catalysts: Nature of the catalytic active sites, ACS Catal. 1 (2011) 54–66.

[14] N. Atar, T. Eren, M.L. Yola, H. Karimi-Maleh, B. Demirdögen, Magnetic iron oxide and iron oxide@-gold nanoparticle anchored nitrogen and sulfur-functionalized reduced graphene oxide electrocatalyst for methanol oxidation, RSC Adv. 5 (2015) 26402–26409.

[15] C.T. Wang, R.J. Willey, Oxidation of methanol over iron oxide based aerogels in supercritical $CO_2$, J. Non-Cryst. Solids 225 (1998) 173–177.

[16] H. Meng, Z. Zhang, F. Zhao, T. Qiu, J. Yang, Orthogonal optimization design for preparation of $Fe_3O_4$ nanoparticles via chemical coprecipitation, Appl. Surf. Sci. 280 (2013) 679–685.

[17] Y.C. Dong, R.G. Ma, M.J. Hu, H. Cheng, C.K. Tsang, Q.D. Yang, Y.Y. Li, J.A. Zapien, Scalable synthesis of $Fe_3O_4$ nanoparticles anchored on graphene as a high-performance anode for lithium ion batteries, J. Solid State Chem. 201 (2013) 330–337.

[18] H. Yin, L. Cui, Q. Chen, W. Shi, S. Ai, L. Zhu, L. Lu, Amperometric determination of bisphenol A in milk using PAMAM–$Fe_3O_4$ modified glassy carbon electrode, Food Chem. 125 (2011) 1097–1103.

[19] F. Vitse, M. Cooper, G.G. Botte, On the use of ammonia electrolysis for hydrogen production, J. Power Sources 142 (2005) 18–26.

[20] S.L. Vot, L. Roué, D. Bélanger, Study of the electrochemical oxidation of ammonia on platinum in alkaline solution: Effect of electrodeposition potential on the activity of platinum, J. Electroanal. Chem. 691 (2013) 18–27.

[21] A. Ciszewski, Catalytic oxidation of methanol on a glassy carbon electrode electrochemically modified by a conductive $Ni^{II}$-curcumin film, Electroanalysis 7 (1995) 1132–1135.

[22] A.B.P. Lever, The phthalocyanines—molecules of enduring value; a two-dimensional analysis of redox potentials, J. Porphyrins Phthalocyanines 3 (1999) 488–499.

[23] Y. Leng, W. Guo, X. Shi, Y. Li, A. Wang, F. Hao, L. Xing, Degradation of Rhodamine B by persulfate activated with $Fe_3O_4$: Effect of polyhydroquinone serving as an electron shuttle, Chem. Eng. J. 240 (2014) 338–343.

[24] D.W. Kim, K.S. Kim, S.J. Park, Synthesis and electrochemical performance of polypyrrole-coated iron oxide/carbon nanotube composites, Carbon Lett. 13 (2012) 157–160.